PCCP

Accepted Manuscript

ROYAL SOCIETY OF CHEMISTRY

www.rsc.org/pccp

Effect of Cationic Head Group on Micellization Behavior of New Amide Functionalized Surface Active Ionic Liquids

Raman Kamboj,[‡] Pankaj Bharmoria,[†] Vinay Chauhan,[‡] Gurbir Singh,[‡] Arvind Kumar,[†] Sukhprit Singh,[‡,]* Tejwant Singh Kang[‡,]*

[‡]*Department of Chemistry, UGC-Centre for Advanced Studies-I, Guru Nanak Dev University, Amritsar-143005, India*

[†]*Academy of Scientific and Innovative Research (AcSIR),* [¶]*Salts and Marine Chemicals Division, CSIR-Central Salt and Marine Chemicals Research Institute, Council of Scientific & Industrial Research (CSIR), G. B. Marg, Bhavnagar-364002, Gujarat, India*

Abstract

Amide functionalized surface active ionic liquids (SAILs), 1-methyl-1-dodecyl pipyridinium chloride, [C_{12}APip][Cl], 1-methyl-1-dodecyl pyrrolidinium chloride, [C_{12}APyrr][Cl], 1-methyl-3-dodecyl imidazolium chloride, [C_{12}Amim][Cl], and 1-methyl-1-dodecyl morpholinium chloride, [C_{12}AMorph][Cl] have been synthesized, characterized and investigated for thermal stability, and micellization behavior in aqueous medium. The introduction of amide moiety in alkyl chain decreased the thermal stability of the functionalized SAILs as compared to non-functionalized SAILs bearing simple alkyl chain. A variety of state of art techniques viz. tensiometry, conductometry, steady-state fluorescence, isothermal titration calorimetry (ITC), dynamic light scattering (DLS) and atomic force microscopy (AFM) have been employed to investigate the micellization behavior. Amide functionalized SAILs have shown much lower critical micelle concentration, *cmc* and better surface active properties as compared to homologous non-functionalized SAILs. Steady-state fluorescence has provided information about *cmc*, aggregation number (N_{agg}) and polarity of cybotactic region of micelle, whereas ITC has provided insights about the thermodynamics of micellization. Furthermore, size and shape of the micelles has been investigated employing DLS and AFM techniques.

To whom correspondence should be addressed:

e-mail: tejwantsinghkang@gmail.com; sukhprit@gmail.com Tel: +91-183-2258802-Ext-3206

1. Introduction

The protection of the environment from detrimental effects of industrial pollution has become a vital challenge, where replacement of conventional volatile organic solvents by relatively greener solvents such as ionic liquids (ILs), is expected to play an important role.[1] ILs are a class of organic salts which are liquid around or below 100 °C, and exhibits unique physico-chemical properties such as negligible vapors pressure, high conductivity, high thermal stability, non-flammability and recyclability etc.[2-6] A variety of ILs have been tested in different avenues of scientific research, for example, in organic synthesis, catalysis, preparation of nanostructured materials, separations and extractions, and in electrochemical devices.[7,8] The large number of ILs, which can possibly be synthesized by judicious choice of cation, anion, and alkyl chain length of cation or anion is of huge importance in targeted synthesis of ILs for specific applications.[9-12]

One of the important class of ILs is surface active ionic liquids (SAILs), which are structurally equivalent to conventional ionic surfactants comprising hydrophobic alkyl chain appended to ionic head group and the counterion.[13] The studies concerning micellization behavior of SAILs in aqueous medium or even in short chain in ILs as base solvents is gaining momentum at high speed.[14-16] Till date, a variety of SAILs have been investigated for their self-assembling behavior in aqueous medium.[14-35] In some reports, the affect of ILs in modifying the properties of self-assembled structures of conventional ionic surfactants or lipids in aqueous medium have also been reported where IL has shown to act as electrolyte of co-surfactant depending on the nature of constituent ions of IL.[36,37] SAILs based on 1-alkyl-3-methylimidqazolium cation ($[C_nmim]^+$) are at the forefront of such studies.[15-25] Some complex SAILs, $[C_nmim][C_mH_{2m+1}SO_3]$, based on $[C_nmim]^+$ and n-alkylsulfate anion, $[C_mH_{2m+1}SO_3]^-$, exhibiting lower critical micelle concentration (*cmc*) and better surface activity have been reported.[23,24] Wang *et al.*, have investigated the effect of counterions on

the micellization behavior of $[C_8mim][X]$ (X = [Cl]$^-$ or [Br]$^-$, [NO$_3$]$^-$, [CH$_3$COO]$^-$,[CF$_3$COO]$^-$, [CF$_3$SO$_3$]$^-$, and [ClO$_4$]$^-$) in aqueous medium.[26] In the same article, the effect of nature of the cationic head group have been investigated by comparing the micellization behaviour of 1-octyl-3-methylimidazolium bromide, $[C_8mim][Br]$, 1-octyl-4-methylpyridinium bromide, 4m-$[C_8pyr][Br]$ and 1-methyl-1-octyl pyrolidinium bromide, $[C_8mpyrr][Br]$.[26] The hydrophobicity and steric hindrance of the cations as well as the binding strength of the cations with the counterions have been suggested to play an important role in governing the micellization behavior. Similarly, the influence of cationic ring types on the *cmc* of the SAILs, 1-dodecyl-3-methylpyridinium bromide, $[C_{12}mpy][Br]$, 1-methyl-1-doedecylpiperidinium bromide, $[C_{12}mpip][Br]$, and 1-methyl-1-dodedcylpyrrolidinium bromide, $[C_{12}mpyrr][Br]$ in aqueous solutions have been well investigated by Blesic *et al*.[27] It has been suggested that the micellization behavior of SAILs can be modulated and controlled by changing the hydrophobicity/hydrophilicity, size and polarizability of the head group.

On the other hand, besides the nature of cationic head group or anion, alkyl chain of constituent ion of SAILs is another key moiety which can be functionalized by incorporating specific functional groups such as hydroxyl, ether, ester or amide groups, expected to alter the micellization behavior. In this regard, it has been shown that long chain *β*-hydroxy-*γ*-alkyloxy-*N*-methylimidazolium SAILs bearing hydroxyl group[28] and COOH-functionalized imidazolium based SAILs[29] posses lower *cmc* and superior surface activity as compared to homologous non-functionalized SAILs. Hereafter, SAILs bearing simple alkyl chain will be called as non-functionalized SAILs. Further, the imidazolium based ILs appended with ether or polyether side chain have been shown to be less toxic as compared to non-functionalized SAILs.[30] Garcia *et al*., synthesized ester functionalized imidazolium and pyridinium based ILs, and investigated their antimicrobial activity and micellization behavior in aqueous medium.[31] Very recently, we have reported the effect of alkyl chain length on the

micellization behavior of amide functionalized morpholinium based SAILs, 1-methyl-1-alkyl morpholinium bromide, $[C_nAMorph][Br]$ where $n = 8$, 12 and 16 in aqueous medium where amide group has been found to affect the micellization behavior positively.[32] Similarly amide functionalized pyridinium based SAILs has also been investigated for their micellization behavior using tensiometry only.[33] However, the novel aspect of the present work lies in the fact that the studies on micellization behavior of functionalized SAILs have started recently and there exists no detailed report on the effect of cationic head groups on the micellization behavior of amide functionalized SAILs. Further none of the amide functionalized SAIL has been reported for its micellization behavior except that based on morpholinium cation, that too with chloride as counterion.[32] The findings of this work have been compared with that reported for homologous non-functionalized or functionalized SAILs and conventional cationic surfactants.

Pursuant to continued research in this area,[32,34,35] herein we report the synthesis and micellization behavior of four new amide functionalized SAILs, 1-(2-(dodecylamino)-2-oxoethyl)-1-methylpiperidin-1-ium chloride (1-methyl-1-dodecyl pipyridinium chloride $[C_{12}APip][Cl]$), 1-(2-(dodecylamino)-2-oxoethyl)-1-methylpyrrolidin-1-ium chloride (1-methyl-1-dodecyl pyrrolidinium chloride), $[C_{12}APyrr][Cl]$, 3-(2-(dodecylamino)-2-oxoethyl)-1-methyl-1H-imidazol-3-ium chloride (1-methyl-3-dodecyl imidazolium chloride), $[C_{12}AMim][Cl]$, and 4-(2-(dodecylamino)-2-oxoethyl)-4-methylmorpholin-4-ium chloride (1-methyl-1-dodecyl morpholinium chloride), $[C_{12}AMorph][Cl]$ in aqueous medium. The characteristic properties of micelle such as critical micelle concentration, (*cmc*), degree of counterion binding, (*β*), thermodynamic parameters of micellization, aggregation number (N_{agg}) and size as well as shape of micelle for investigated SAILs have been obtained and compared with their non-functionalized counterparts, wherever possible. Further, the effect of nature of cationic head group on micellization behavior of amide functionalized SAILs have

been discussed in terms of relative hydrophobicity, van der Waal's volume and extent of binding of counterions to micelle. It is anticipated that this work will add up to the just started research avenue of micellization of functionalized SAILs and will put emphasis on functionalization of alkyl chain with other suitable functional groups to get better surface active properties.

2. Experimental

2.1. *Materials:* Chloroacetyl chloride, 1-aminododecane, *N*-Methyl morpholine, *N*-Methyl piperidine, *N*-Methyl pyrrolidine and *N*-Methyl imidazole, cetylpyridinium chloride ($> 99\%$) was purchased from Sigma-Aldrich and used without further purification. Dichloromethane, acetone and diethyl ether (AR grade) were purchased from SD Fine-Chem Ltd., Mumbai, India. Pyrene was purchased from Sigma Aldrich and used after recrystallization from ethanol. The SAILs under investigation have been synthesized as discussed in Section 3.1.

2.2. Methods

2.2.1. Melting Point and Thermal stability Measurements: Differential scanning calorimetry was performed using Mettler Toledo DSC822 thermal analyzer at a scan rate of $10\ ^0C\ min^{-1}$ to get the melting point of the investigated SAILs. The thermal stability of the prepared SAILs was judged by employing thermogravimetric analysis (TGA) which was performed on a TGA/SDT A851 Mettler Toledo thermogravimeter under N_2 atmosphere at a heating rate of $10\ °C\ min^{-1}$ in the temperature range of 30 to 400 °C.

2.2.2. Tensiometry: Surface tension was measured using a Data Physics DCAT II automated tensiometer employing the Wilhelmy plate method at 298.15 K. A Julabo thermostat has been used to control the temperature of the measurements within the accuracy of ±0.1 K. The tensiometer was calibrated using triple distilled water. Before each measurement, Wilhelmy plate was cleaned and dried very carefully to avoid any

contamination. The data was obtained in triplicate and found to be accurate within ± 0.1 mN m^{-1}.

2.2.3. ***Conductometry:*** Conductivity was measured on an Equip-Tronics auto temperature conductivity meter, model EQ661 equipped with a cell of unit cell constant at 298.15 K. Prior to the measurements, the conductivity cell was calibrated using aqueous solutions of KCl of different concentrations. Temperature of the measurement was controlled within the accuracy of ±0.1 K using a water thermostat. Measurements were performed in triplicate with an uncertainty of less than 0.6%.

2.2.4. ***Isothermal titration calorimetry:*** The calorimetric measurements were performed to determine the enthalpy changes occurring during the micellization, using MicroCal ITC200 microcalorimeter, equipped with an instrument controlled Hamilton syringe having a volume capacity of 40 μL. The titration was done automatically by adding 2 μL aliquots of known concentrated stock solution of SAILs into the sample cell containing 200 μL of water with continuous stirring at 600 rpm. The enthalpy change at each addition was determined and plotted against concentration of SAILs to obtained various thermodynamic parameters such as standard free energy (ΔG_m^0), standard enthalpy (ΔH_m^0), and standard entropy (ΔS_m^0) of micellization.

2.2.5. ***Steady-state fluorescence:*** Steady-state fluorescence measurements were carried out using a PerkinElmer LS-55 spectrophotometer, equipped with a built-in temperature controller, maintained at 298.15 K. An excitation and emission slit width of 2.5 nm, each, was used and the emission spectra were measured in the wavelength of range of 350-500 nm using an excitation wavelength of 334 nm. The ratio of the intensities of the first to third vibronic peaks (I_1/I_3) of pyrene fluorescence was used to obtain the *cmc* of the SAILs and to estimate the micropolarity of micelle as sensed by pyrene. Pyrene and cetylpyridinium chloride (CPC) were used as the fluorescence probe and quencher, respectively, for

fluorescence quenching experiments. The concentration of pyrene was kept as 2.0×10^{-6} M to avoid the formation of excimer. All the data were acquired using quartz cuvette having a path length of 1 cm.

2.3.5. Dynamic light scattering (DLS): Dynamic light scattering measurements were performed using a light scattering apparatus (Zeta-sizer, nano-series, nano-ZS) Malvern Instruments, equipped with a built-in temperature controller having an accuracy of $\pm$ 0.1 K. The aqueous solutions of SAILs were prepared in Millipore water and filtered through a membrane filter (1.0 μm pore size) to avoid presence of dust particles, before measurements. The samples were thermally equilibrated for 10 minutes before each measurement and an average of 30 measurement runs were considered as data. The data was analyzed using the standard algorithms and is reported with an uncertainty of less than 7%.

2.3.6. Atomic Force Microscopy: Atomic force microscopy (AFM) was performed using Ntegra Aura atomic force microscope (NT-MDT, Russia) in semi-contact mode using an NSG-01 silicon probe. Samples were prepared by putting a drop of the sample solution (twice the concentration of *cmc* of respective SAIL) on a thin mica sheet followed by drying in air for 48 hours before measurements.

3. Results and Discussion

3.1. Synthesis and Thermal Stability: Amide functionalized SAILs have been synthesized employing a two-step strategy. The detailed methodology of synthesis and characterization data (NMR and mass) are provided in Annexure 1 (supporting information). In brief, first, 2-chloro-*N*-dodecylacetamide was synthesized by reacting 1-aminododecane and chloroacetyl chloride utilizing reported procedure with some modifications.[38,39] Following that 2-Chloro-*N*-dodecylacetamide was subsequently quaternized by different heterocyclic amines (*N*-methyl piperidine, *N*-methyl pyrrolidine, *N*-methyl imidazole and *N*-methyl morpholine) in

the second step to get amide functionalized SAILs. Scheme 1 shows the molecular structure of investigated SAILs.
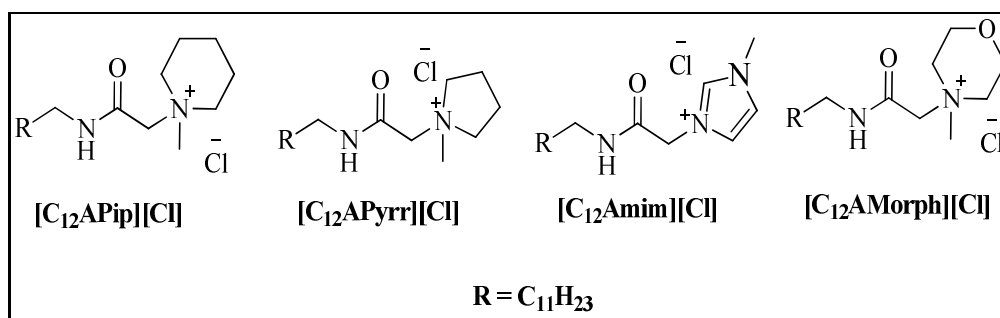
Scheme 1. Molecular structures of synthesized amide functionalized SAILs

The synthesized SAILs have been characterized for their thermal properties such as m*elting point and thermal stability.* Figure 1 A and B shows the differential scanning calorimetry (DSC) thermograms and thermgravimetric (TGA) profiles for the investigated SAILs, respectively.
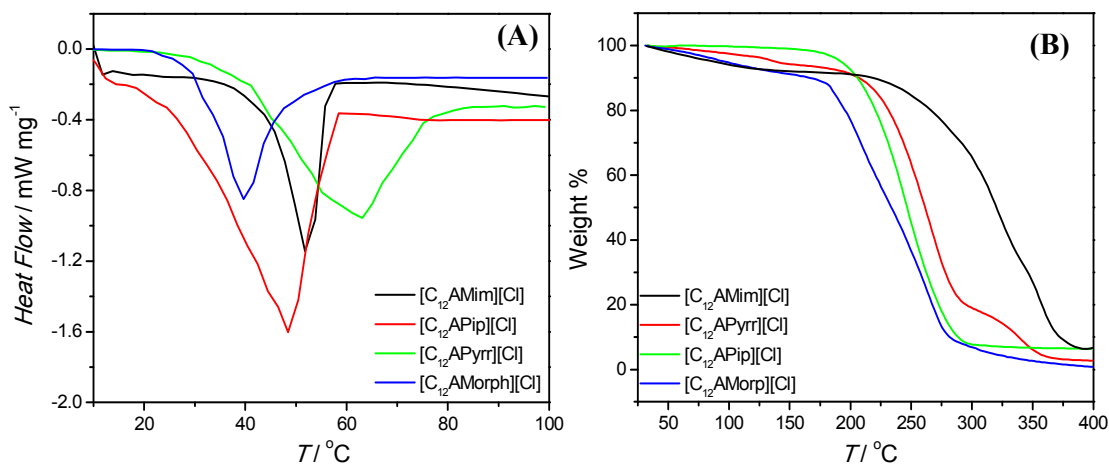
Figure 1 (A,B): (A) Differential scanning calorimetry thermograms; and (B) thermogravimetric analysis profiles (TGA) of various investigated SAILs.

DSC thermograms have established that the melting point of investigated SAILs in the range of 40 to 63 $^{\circ}$C which categories the investigated SAILs in the category of ILs. The temperature of onset (T_{onset}) of decomposition is obtained as the intersection of baseline weight, either from the start of the experiment and the tangent of the weight vs. temperature curve as the decomposition occurs.[40] T_{onset} for the amide-functionalized SAILs have been

investigated and compared with non-functionalized $[C_{12}mim][Br]$[41], $[C_{12}Pyr][Br]$[42] and ester-functionalized[31] $[C_{12}Emim][Br]$, $[C_{12}EPyr][Br]$ SAILs in Table S1 (Supporting information). It can be seen from Table S1 (Supporting information) that non-functionalized SAILs exhibit better thermal stability as compared to amide and ester functionalized SAILs. Values of T_{onset} for investigated SAILs $[C_{12}APip][Cl]$, $[C_{12}APyrr][Cl]$, $[C_{12}Amim][Cl]$ and $[C_{12}AMorph][Cl]$, have been observed as 196, 211, 218, and 182 °C, respectively. The slight variation in T_{onset} values for investigated SAILs can be attributed to the nature of cationic headgroup structure. The slightly higher thermal stability of the $[C_{12}APip][Cl]$ as compared to that of $[C_{12}AMorph][Cl]$ can be assigned to the presence of ether linkage in the cationic morpholinium head group. It has been observed that the presence of ether group caused a negative effect on the thermal stability and the thermal decomposition temperature decreased with the increasing number of ether groups in cation.[43] Further, SAILs viz. $[C_{12}APyrr][Cl]$ and $[C_{12}Amim][Cl]$ exhibit better thermal stability as compared to $[C_{12}APip][Cl]$ or $[C_{12}AMorph][Cl]$. From this data, it has been inferred that with decrease in the size of cationic head group, there is slight increase in the T_{onset} of respective SAIL.

3.2. Surface Active Behavior and Micellization: Surface tension measurements have been performed to investigate and evaluate the surface active properties of the investigated SAILs in their aqueous solutions. Figure 2 shows the variation of the surface tension (γ) in aqueous solutions of investigated SAILs at 298.15 K as a function of ln of concentration (C). The surface tension decreased initially with increasing concentration of SAILs, and then reached a plateau region, after which a constant value (γ_{cmc}) has been observed. The concentration of respective SAIL corresponding to constant value of γ signifies the critical micelle concentration (*cmc*). The obtained values of *cmc* are provided in Table 1. For different investigated SAILs, *cmc* varies in the order: $[C_{12}APip][Cl]$ < $[C_{12}APyrr][Cl]$ <

$[C_{12}Amim][Cl] < [C_{12}AMorph][Cl]$. The variation in *cmc* can be related with the relative

hydrophobicity or van der Waal's volume of cationic head group.
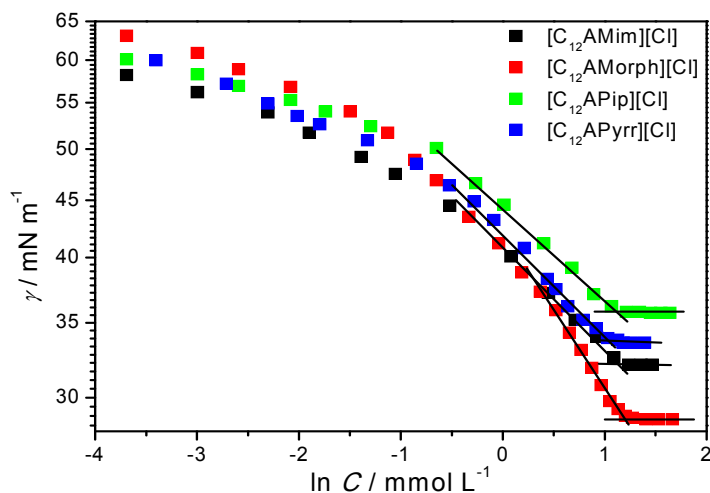
Figure 2: Variation of surface tension, γ, in aqueous solutions of various amide functionalized SAILs as a function of ln of concentration at 298.15 K. The break point in the γ *vs. ln C* profiles indicates the *cmc*.

The hydrophobicity of the cationic head groups of investigated SAILs follows the order:

$[C_{12}APip][Cl] > [C_{12}APyrr][Cl] > [C_{12}Amim][Cl] > [C_{12}AMorph][Cl]$[44] and the

corresponding van der Waal's volume follows the order: $[C_{12}APip][Cl] > [C_{12}AMorph][Cl] >$

$[C_{12}Amim][Cl] \approx [C_{12}APyrr][Cl]$. From this, it is inferred that the *cmc* is mainly affected by

the hydrophobicity of the cationic head group where *cmc* increases with decreasing

hydrophobicity of the cationic head group. The *cmc* values of the investigated SAILs have

been found to be 3-4 fold lower as compared to previously reported non-functionalized

$[C_{12}mim][X]$,[45,46] $[C_{12}Pyr][X]$[47,48] (X = Br and Cl), $[C_{12}mPip][Br]$[49], $[C_{12}mPyrr][Br]$[50] SAILs

and comparable to that of ester functionalized $[C_{12}Emim][Br]$, $[C_{12}EPyr][Br]$[31] SAILs. This

contrasting behavior can be assigned to be presence of amide moiety in the alkyl chain, prone

to take part in *H*-bonding. The obtained values of γ_{cmc} for the investigated SAILs are provided

in Table 1. γ_{cmc} decreases following the order: $[C_{12}APip][Cl] > [C_{12}APyrr][Cl] >$

$[C_{12}Amim][Cl] > [C_{12}AMorph][Cl]$ signifying that with an increase in hydrophobicity of the

cationic head group, the efficiency of the SAILs to reduce the surface tension increases. The

trend of decrease in surface tension attained at *cmc* for these SAILs can also be explained on

the basis of cmc/C_{20} ratio.

Table 1. Surface properties of SAILs as determined by surface tension, conductivity, fluorescence and isothermal titration calorimetry measurements.

SAIL	cmc^a mM	cmc^b mM	cmc^c mM	cmc^d mM	γ_{cmc} mN/m	Π_{cmc} mN/m	$10^6\Gamma$ mol/m^2	A_{min} Å^2	$10^4 C_{20}$	pC_{20}	cmc^a/C_{20}	ΔG°_{ads} kJ/mol
[C$_{12}$APip][Cl]	3.10	5.20	3.68	4.05	35.6	36.4	1.65	100	3.0	3.51	10.3	-59.7
[C$_{12}$APyrr][Cl]	3.25	5.45	4.10	3.40	33.9	38.1	1.61	103	1.6	3.79	20.3	-56.1
[C$_{12}$Amim][Cl]	3.43	5.80	5.14	4.55	32.2	39.8	1.47	113	1.5	3.82	22.9	-62.7
[C$_{12}$AMorph][Cl]	3.85	6.64	5.60	4.82	28.7	43.3	1.93	86	2.2	3.65	17.5	-58.4

[a]Surface tension measurements; [b]Electrical conductivity measurements; [c]isothermal titration calorimetry; [d]Fluorescence measurements

A larger cmc/C_{20} ratio signifies the greater tendency of the SAIL to reduce surface tension of

the system,[51] where C_{20} is the minimum concentration of the surfactant required to reduce the

surface tension of solvent by 20 mN m^{-1}. As can be seen from Table 1, cmc/c_{20} ratio increases

following the order: [C$_{12}$APip][Cl] < [C$_{12}$AMorph][Cl] < [C$_{12}$APyrr][Cl] < [C$_{12}$Amim][Cl].

The order is just reverse to that observed for variation of γ_{cmc}, with an exception of

[C$_{12}$AMorph][Cl]. From Table 1, it can be seen that a relative increase in C_{20} for

[C$_{12}$AMorph][Cl] lowers the cmc/C_{20} ratio. An increase in C_{20} for [C$_{12}$AMorph][Cl] can be

assigned to the presence of highly electronegative oxygen atom on cationic head group which

is expected to cause electrostatic repulsions between cationic head groups at air/solution

interface initially in low concentration regime, leading to higher C_{20}. The values of C_{20} vary

in line with the variation in van der Waal's volume indicating that C_{20} is mainly controlled by

the size of the cationic head group. Therefore, it is concluded that the adsorption at

air/solution interface is controlled, both by hydrophobicity and van der Waal's volume of the

cationic head group, where van der Waal's volume is dominating at lower concentration of

SAILs and the hydrophobicity dominates near the *cmc*. The presence of amide group in

investigated SAILs leads to significant increase in the cmc/C_{20} ratio as compared to non-functionalized homologues SAILs.[51]

Two other important parameters judging the micellization are the effectiveness of surface tension reduction, π_{cmc} and the adsorption efficacy, pC_{20}, which can be deduced from the measured surface tension data as following:[51]

$$\pi_{cmc} = \gamma - \gamma_{cmc} \tag{1}$$

and

$$pC_{20} = -log C_{20} \tag{2}$$

where γ_o is the surface tension of pure solvent and γ_{cmc} is the surface tension of the solution at the *cmc*. The obtained values of Π_{cmc} and pC_{20} are provided in Table 1. Variation of Π_{cmc} with varying cationic head group is in line with the variation in γ_{cmc}. Π_{cmc} values for investigated SAILs are higher than that of non-functionalized SAILs $[C_{12}mPip][Br]$,[49] $[C_{12}mPyrr][Br]$[50] and conventional cationic surfactants[51-54] indicating the higher ability of investigated SAILs over the non-functionalized SAILs and conventional cationic surfactants to reduce the surface tension.

The maximum surface excess concentration at the air-solution interface Γ_{max}, has been calculated by applying the Gibbs adsorption isotherm:[51]

$$\Gamma_{max} = -\frac{1}{2.303nRT} \left(\frac{d\gamma}{d\log C} \right)_T \tag{3}$$

Where R is the gas constant, T the absolute temperature in K, γ the surface tension, C the concentration of surfactant. The value of n is 2 as there is one counter ion associated with one ionic head group. The minimum area occupied per surfactant molecule (A_{min}) at the air-solution interface has been deduced using the following equation:[51]

$$A_{min} = 1/N\Gamma_{max} \tag{4}$$

where N is Avogadro's number. Both Γ_{max} and A_{min} reflects the surface arrangement of given surfactant at air/solution interface. As can be seen from Table 1, the values of Γ_{max} decreases following the order: $[C_{12}AMorph][Cl] > [C_{12}APip][Cl] > [C_{12}APyrr][Cl] > [C_{12}Amim][Cl]$ whereas A_{min} increases in reverse order. The order of decrease in Γ_{max} or increase in A_{min} is in corroboration with the variation in γ_{cmc} values indicating the relatively compact packing of $[C_{12}AMorph][Cl]$ over other investigated SAILs at the air/solution interface. Further, all the investigated SAILs have been found to possess lower Γ_{max} and a higher A_{min} values as compared to previously reported non-functionalized $[C_{12}mim][X]$[45,46] (X = Br and Cl), $[C_{12}Pyr][Br]$,[47,48] $[C_{12}mPip][Br]$,[49] $[C_{12}mPyrr][Br]$[50] SAILs, and ether functionalized $[C_{12}Emim][Br]$,[31] $[C_{12}EPyr][Br]$[31] SAILs. A lower value of Γ_{max} and a higher value of A_{min} signify a loose packing of the molecules of respective SAILs at the air/solution interface.[48] This loose packing can be assigned to the varying orientation of the cationic head group as a consequence of H-bonding (intermolecular and intramolecular) of the amide moiety. Such behavior is assumed to be originated from dominance of intermolecular H-bonding between amide moiety and the water over the intermolecular H-bonding between amide groups of surfactant ions at air/solution interface. The nature of head group seems to be the key factor in deciding the surface properties of these amide functionalized SAILs in parallel with the earlier reports establishing that the hydrophilic head group size is a dominant factor in governing the adsorption of SAILs at air/solution interface, however the role of relative hydrophobicity of cationic head group cannot be ruled out, completely.[51]

3.3. Micellization in Bulk and Degree of Counter-ion Binding: Micellization of SAILs in bulk has been investigated by electrical conductivity measurements. Figure 3 (A) and (B) depicts the variation in specific conductivity, (κ) and molar conductance (Λ_m), respectively as a function of concentration (C) of SAILs in aqueous medium at 298.15 K. It can be observed that, for each SAIL, the κ vs. C profiles (Figure 3A) can be well fitted into two straight lines

with different slopes, leaving a break point (marked red). The break in the κ versus C plot originates from the micellization of surfactant ions, and the concentration corresponding to the break point is *cmc*, the values of which are provided in Table 1.[55]
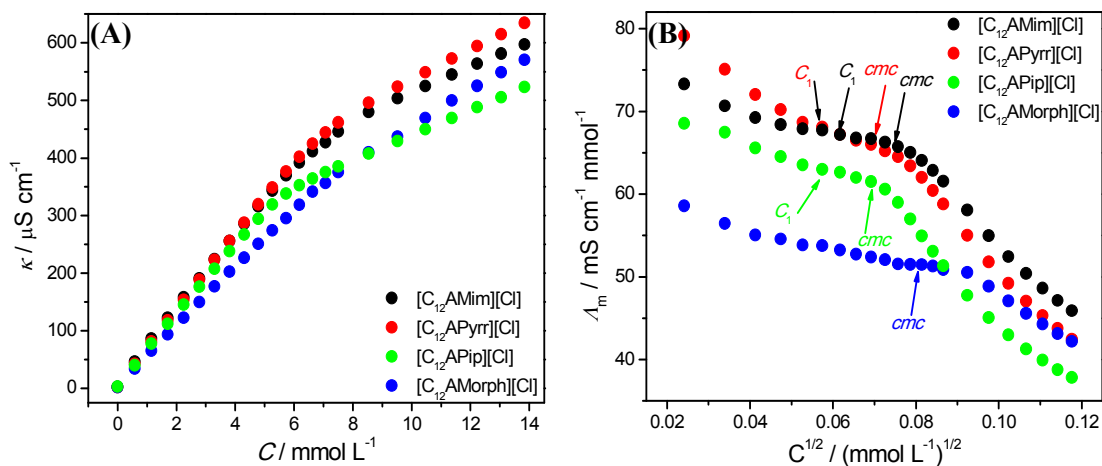
Figure 3(A,B): Variation of (A) specific conductance; and (B) molar conductance in aqueous solutions of various amide functionalized SAILs as a function concentration at 298.15 K.

The obtained values of *cmc* as determined by conductivity method have been found to be higher than that obtained from surface tension measurements, as different techniques senses the different stages of micellization. However the dependence of *cmc* on nature of cationic head group of investigated SAILs follows the same trend as observed from tensiometry. As can be seen from Figure 3 A, the variation of κ with C follows a relatively higher and lower slope before and after micellization, respectively. Below *cmc*, higher mobility of free surfactant ions and counterions leads to higher conductivity, whereas a decrease in mobility upon micellization with a fraction of bound counterions leads to relative decrease in conductivity. Therefore, the change in slopes of κ with C below and above *cmc* is frequently used to get the fraction of bound counterions to micelle. The degree of counterion dissociation (α) has been obtained as the ratio of slopes (S_2/S_1) of κ with C profiles above (S_2) and below (S_1) *cmc*. The degree of counter ion binding (β) to micelles can be calculated from α and is equal to $1 - \alpha$.[51,56] The calculated values of β are listed in Table 2. The values of β for

the investigated SAILs follow the order: $[C_{12}APip][Cl] > [C_{12}AMorph][Cl] > [C_{12}Amim][Cl] > [C_{12}APyrr][Cl]$.

Table 2. Degree of counterion binding, (β) and standard free energy of micellization,(ΔG_m^o) from conductivity measurements, standard free energy of micellization,(ΔG_m^o), standard enthalpy micellization,(ΔH_m^o), and standard entropy of micellization,$(T\Delta S_m^o)$ from isothermal calorimetry measurements, polarity indicator (I_1/I_3) for cybotactic region of pyrene in micelles and aggregation number (N_{agg}) of micelle of various IL surfactants obtained from steady-state fluorescence measurements at 298.15 K.

SAIL	β [a]	ΔG_m^{o} [a]	ΔG_m^{o} [b]	ΔH_m^{o} [b]	$T\Delta S_m^{o}$ [b]	I_1/I_3 [c]	N_{agg} [c]
$[C_{12}APip][Cl]$	0.64	-37.7	-39.1	-1.6	37.5	1.17	49
$[C_{12}APyrr][Cl]$	0.42	-32.5	-33.4	-1.4	32.0	1.07	74
$[C_{12}Amim][Cl]$	0.57	-35.7	-36.1	-1.5	34.6	1.11	71
$[C_{12}AMorph][Cl]$	0.61	-36.0	-36.7	-3.1	33.6	1.14	66

[a]Electrical conductivity measurements; [b]isothermal titration calorimetry; [c]Fluorescence measurements. For determination of N_{agg}, concentration of the respective SAILs was $\approx$ 13.8 mmol L^{-1}.

Although both the hydrophobicity and size of the cationic head group along with their tendency to bind to counterions affects the β, however it seems that here the size of the cationic head group is the dominating factor in controlling the β, where β decrease with decrease in size of the cationic head group. The Λ_m vs. C profiles (Figure 3 B) can be used to interpret the formation of premicelles. The relative change in slope in variation of Λ_m in the dilute concentration regime marked as C_1 where there is onset of pre-micellization and between C_1 and *cmc* has been used to estimate the extent of formation of premicelles in investigated SAILs. With the exception of $[C_{12}AMorph][Cl]$, all the investigated SAILs have found to form some sort of premicellar structures, being maximum in the case of $[C_{12}APyrr][Cl]$ as indicated by maximal change in slope for observed Λ_m. Further the pseudophase model of micellization has been applied to get the value of standard free energy of micellization (ΔG_m^o) using the following equation:[51]

$$\Delta G_m^{\circ} = (1+\beta)RT \ln X_{cmc} \qquad\qquad 5$$

where R is the gas constant, T is temperature in K, X_{cmc} is *cmc* in mole fraction and β is degree of counterion binding. The calculated values of ΔG_m^0 are given in Table 2. Negative values of ΔG_m^o for all the SAILs indicate the spontaneity of micellization. On comparison, it has been observed that the magnitude of ΔG_m^0 decreases with decrease in size of the cationic head group. Further, the Gibbs free energy of adsorption (ΔG°_{ads}) at the air/solution interface has been calculated using the following equation:[51]

$$\Delta G_{ads}^o = \Delta G_m^o - \frac{\pi_{cmc}}{\Gamma}$$

6

where ΔG_m^o is standard free energy of micellization calculated from conductivity measurements (section 3.2). For all the investigated SAILs, higher magnitude of ΔG_{ads}^o as compared to ΔG_m^o indicate that adsorption at air/solution interface is more spontaneous than micellization in bulk.

3.4. Thermodynamics of Micellization: The thermodynamics of micellization has been investigated by isothermal titration calorimetry (ITC) at 298.15 K. Figure 4 (A-D) shows the enthalpograms of different SAILs as a function of concentration. Different types of entahlpograms have been demonstrated for the aqueous surfactant solutions, where degree of counterion binding, molar enthalpy of monomer, molar enthalpy of micelle and aggregation number have been shown to affect the nature of enthalpogram.[57-60] The so called text book type enthalpogram has been observed in the case of [C$_{12}$AMorph][Cl] showing a constant enthalpy change before *cmc* followed by a sharp decrease till a plateau is reached. Both [C$_{12}$AMim][Cl] and [C$_{12}$APip][Cl] have exhibited similar type of enthalpograms with the difference that before *cmc*, a marginal decrease in change in enthalpy has been observed in the case of [C$_{12}$AMim][Cl], whereas a very small increase has been observed in later case with increase in concentration of respective SAIL. After *cmc*, the change in enthalpy decreases exponentially. However, a small exponential decrease in dilute concentration regime followed by exponential increase before *cmc* has been observed in case of

[C$_{12}$APyrr][Cl]. This decrease is assigned to be a consequence of formation of premicelles in this concentration regime. Such behavior has also been observed for [C$_8$AMorph][Br].[32]
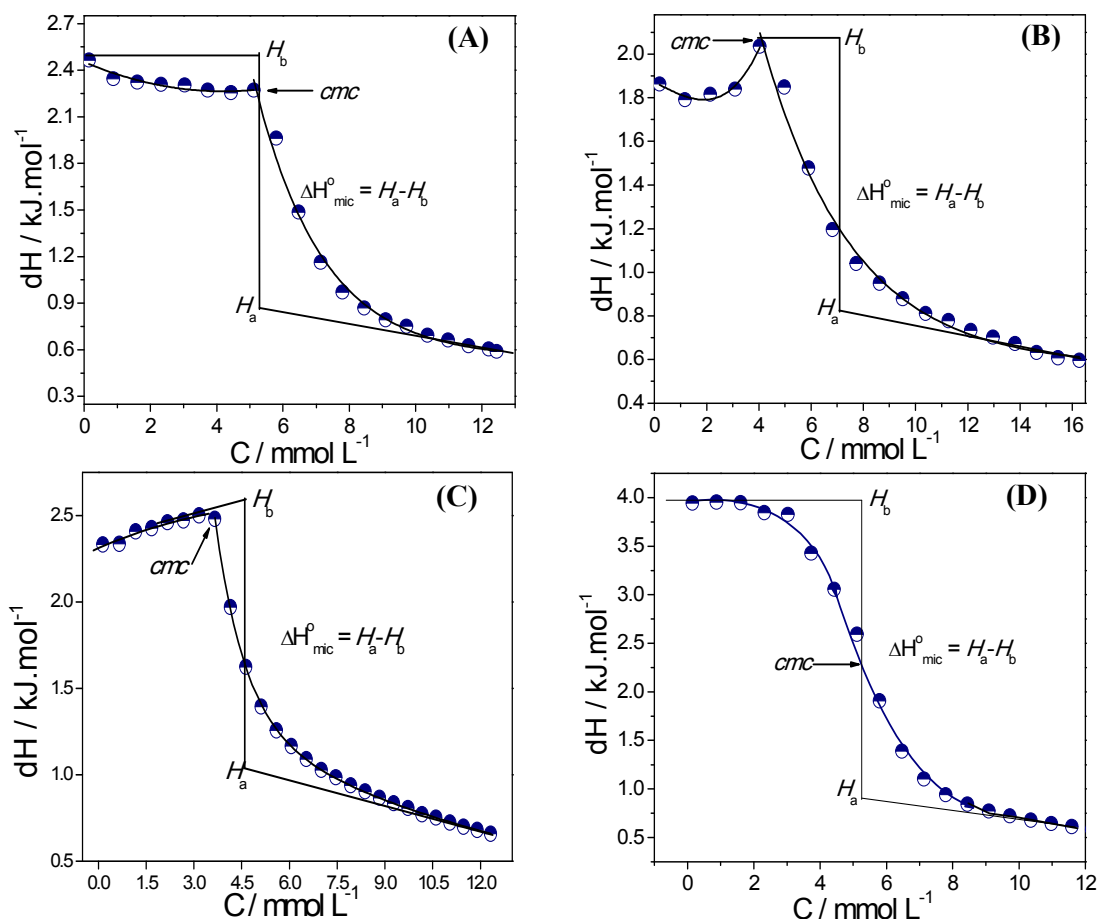
Figure 4 (A-D): Calorimetric profiles of amide functionalized SAILs: (A) [C$_{12}$AMim][Cl]; (B) [C$_{12}$APyrr][Cl]; (C) [C$_{12}$APip][Br] and [C$_{12}$AMorph][Cl] in aqueous solutions at 298.15 K.

The standard enthalpy of micellization (ΔH_m^0), for [C$_{12}$AMorph][Cl] was determined by simple graphical extrapolation method as the sharp transition has been observed in entahlpogram of the respective surfactant. In rest of the cases *i.e.* [C$_{12}$APip][Cl], [C$_{12}$APyrr][Cl] and [C$_{12}$Amim][Cl], the ΔH_m^0 has been determined by analyzing the data according to literature reports,[57-60] as in these systems, the entahlpogram do not show clear sigmoidal features. As can be seen from Figure 4(A and C) the difference between the intercepts of lower and upper concentration domains yielded, ΔH_m^0. As ITC cannot be used

independently to determine the ΔG_m^0, along with the related entropy of micellization (ΔS_m^0). Therefore ΔG_m^0 has been calculated using the *cmc* determined from ITC, and degree of counterion binding, β, obtained by conductivity method, which is equal to a parameter, 1-*p*/*n* used in ITC measurements, (β = 1-p/n), where *p* indicates the charge on micelle and *n* is the aggregation number (N_{agg}) of micelle.[32,60] Further, the Gibbs-Helmolthz equation has been used to obtain the related ΔS_m^0. Table 2 shows the values of thermodynamic parameters of micellization obtained from ITC measurements. The ΔG_m^0 obtained from ITC measurements has been found to be in corroboration with that observed from conductometry within in the limitations of the measurement. ΔH_m^0 for different SAILs follows the order: [C$_{12}$AMorph][Cl] > [C$_{12}$APip][Cl] > [C$_{12}$AMim][Cl] > [C$_{12}$APyrr][Cl] indicating that the maximum enthalpic contribution towards free energy change is in the case of [C$_{12}$AMorph][Cl]. Similarly the entropic contribution to ΔG_m^0 follows the order: [C$_{12}$APip][Cl] > [C$_{12}$AMorph][Cl] > [C$_{12}$AMim][Cl] > [C$_{12}$APyrr][Cl]. Both the β and N_{agg} along with other parameters discussed above have a say in this phenomenon. Other factors which are expected to affect the ΔH_m^0 by affecting β and N_{agg} are hydrophobicity and van der Waal's volume of cationic head group as the extent of hydration and steric effect of the cationic group will affect the overall enthalpy change during the course of micellization. The order of variation in ΔH_m^0 as well as for $T\Delta S_m^0$ for different SAILs is more close to that of variation in van der Waal's volume of cationic head group (section 3.1). As the change in enthalpy depends on many interdependent factors, further discussion in this regard will be problamistic.[57] It has been observed that the micellization of the investigated SAILs is an entropy driven phenomenon where the contribution of enthalpy change is very less. The enthalpy change on micellization is mainly contributed by hydrophobic interactions between the alkyl chains releasing hydrating water molecules (exothermic) and electrostatic interactions between the surfactant head groups and the counterions (endothermic) whereas electrostatic repulsions between surfactant head

groups contribute exothermically.[61,62] As β for investigated SAILs is rather good, it suggests the dominance of endothermic contribution via electrostatic attraction between surfactant head groups and counterions towards total enthalpy change. Further it is expected that due to the presence of amide group, it will be difficult to release all of the hydrating water molecules by surfactant ions upon micellization leading to relatively less exothermic contribution towards total enthalpy change.

3.5.　Micellization Behavior and Aggregation Number: Pyrene monomer fluorescence emission is useful for monitoring the self-aggregation of amphiphiles in aqueous solution. The emission spectra of pyrene show five emission bands, where the intensity of first band is enhanced in a polar environment, while the intensity of third band is not much sensitive to the surrounding environment. Thus, the ratio of the intensity of the first to the third vibronic band (I_1/I_3), not only probes the micropolarity of the surfactant aggregates, but is also used to obtain the *cmc* of the surfactants in aqueous solution as preferential dissolution of pyrene in hydrophobic regions of micelle decreases the I_1/I_3 on micellization.[63] Figure 5(A) represents the variations of I_1/I_3 of pyrene as a function of concentration of respective SAILs. The mid-point of the transition has been considered as *cmc*, and is provided in Table 1.
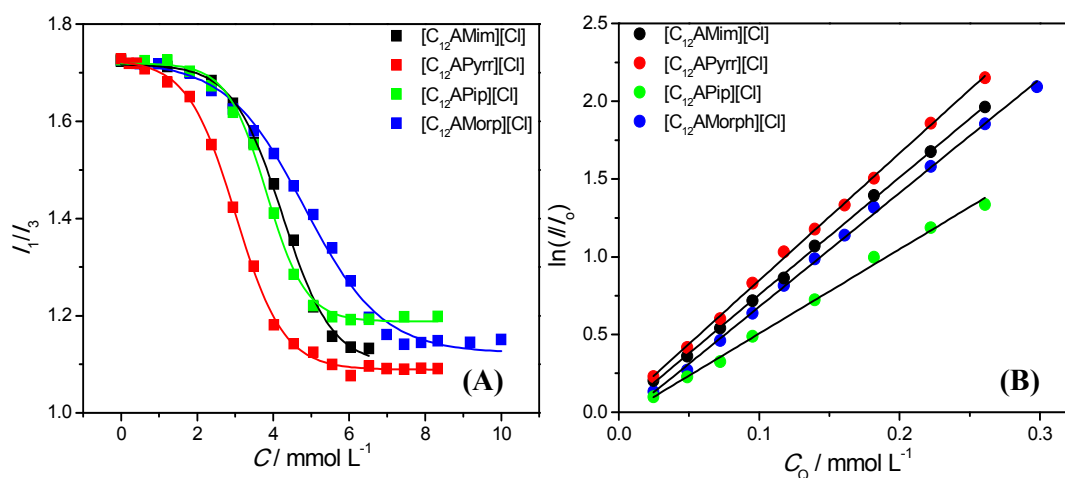
Figure 5 (A,B): Variation of (A) I_1/I_3 of pyrene emission as a function of concentration of different SAILs; and (B) variation of $\ln(I/I_o)$ as a function of concentration of quencher, C_Q. Lines in Figure 5(A) and 5 (C) are sigmoidal and linear fits of the data, respectively with Adj. $R^2 > 0.997$.

The *cmc* values obtained from fluorescence measurements are in accordance with those

obtained from other techniques with an exception of [C$_{12}$APyrr][Cl] which seems to be due to

formation of premicelles as revealed by conductivity and ITC measurements. The value of

I_1/I_3 (Table 2) in micelles of various SAILs follows the order: [C$_{12}$APip][Cl] <

[C$_{12}$AMorph][Cl] < [C$_{12}$AMim][Cl] < [C$_{12}$APyrr][Cl] indicating the decreased compactness

of micelle while going from [C$_{12}$APip][Cl] to [C$_{12}$APyrr][Cl]. The order is also supported by

the *β* which follows the reverse order as compared to variation in I_1/I_3. The observed order of

compactness of micelle is very much explainable on the basis of van der Waal's volume of

cationic head group suggesting that more bulky is the cationic head group, more compact the

micelle is.

The aggregation number (N_{agg}) of the micelles has been determined by steady-state

fluorescence quenching experiments using pyrene and cetylpyridinium chloride as

fluorescent probe, and quencher, respectively. The micelle aggregation number was

determined by using equation 7, as per the method described by Turro-Yekta:[64]

$$\ln\left(\frac{I_o}{I}\right) = \frac{N_{agg}C_Q}{C_s - cmc} \qquad\qquad 7$$

where I_o and I are the fluorescence intensities of pyrene in the absence and presence of the

quencher at a specific wavelength, C_Q and C_s are the molar concentrations of the quencher

and investigated SAIL, respectively. Figure 5(B) shows the variation of $\ln(I_o/I)$ of pyrene

fluorescence as a function of the concentration of the quencher [C_Q] in micellar solutions of

investigated SAILs. The obtained N_{agg} for different SAILs is given in Table 2, and follows the

order: [C$_{12}$APyrr][Cl] < [C$_{12}$Amim][Cl] < [C$_{12}$AMorph][Cl] < [C$_{12}$APip][Cl], which is in

accordance with the size of micelles determined by dynamic light scattering (DLS)

measurements as discussed in next section. It can be observed that N_{agg} increases with

increase in bulkiness of cationic head group similar to that observed for variation of I_1/I_3.

However, the results are contrary to those reported for non-functionalized SAILs bearing same cationic head groups, where it was observed that higher N_{agg} was favored by increased hydrophobicity of the cationic head group.[26] The discrepancy can be assigned to the presence of amide functionality which is expected to counterbalance the steric and electrostatic repulsions between the bulky cationic head groups by formation of intermolecular *H*-bonding in micelle in bulk. The existence of *H*-bonding between the amide protons of SAILs in micelles has been probed by ^{1}H NMR spectroscopy exploiting the temperature dependence of chemical shift, δ. The sign and magnitude of temperature coefficient ($\Delta\delta/\Delta T$) gives an idea about type and strength of *H*-bonding.[65] The temperature coefficient in micellar solutions of [C$_{12}$Amim][Cl] has been shown in Figure S1 (supporting information) as a representative. The comparatively less negative value *i.e.* -1.2 ppb/K of $\Delta\delta/\Delta T$ for amide proton indicates the presence of strong intermolecular H-bonding between amide protons of neighboring SAIL molecules in micelle. On the other hand, $\Delta\delta/\Delta T$ value of -6.0 ppb/K for acidic proton present between two N-atoms at imidazolium ring indicates the presence of strong solute-solvent inter-molecular *H*-bonding. The variation in β is also in accordance with the trend observed for N_{agg} which indicates the role of hydrophobicity of cation, it can be believed that in the investigated SAILs, the relative dominance of hydrophobicity, polarizability and bulkiness of the cationic head group controls the micellar properties. The N_{agg} of these SAILs has been found to be higher as compared to non-functionalized SAILs, [C$_{12}$mim][X][45,46] (X = Br and Cl) and [C$_{12}$mPyrr][Br][50] and this difference may be attributed to the presence of amide linkage in the alkyl chain where intermolecular *H*-bonding is expected to stabilize the micelles.

3.6. Size and Morphology of the Aggregates:

Dynamic light scattering (DLS) and atomic force microscopy (AFM) has provided insights into the size distribution as well as shape of the micelles of investigated SAILs in aqueous

solutions, respectively. Figure 6 shows the intensity weighed size distribution profiles of

micelles of investigated SAILs. Two size distributions corresponding to smaller and larger

hydrodynamic diameter (D_h) has been observed. The smaller D_h is assigned to be the diameter

of micelle and the larger D_h is assigned to micellar agglomerates. Further, it has been

established that a particles twice the size of smaller particle scatters 64 times more light.[66]

Therefore, considering the higher scattering intensity by smaller micelles as compared to

larger micellar agglomerates (Figure 6), it can be said that the number of smaller micelles is

much more as compared to that of larger micellar agglomerates.
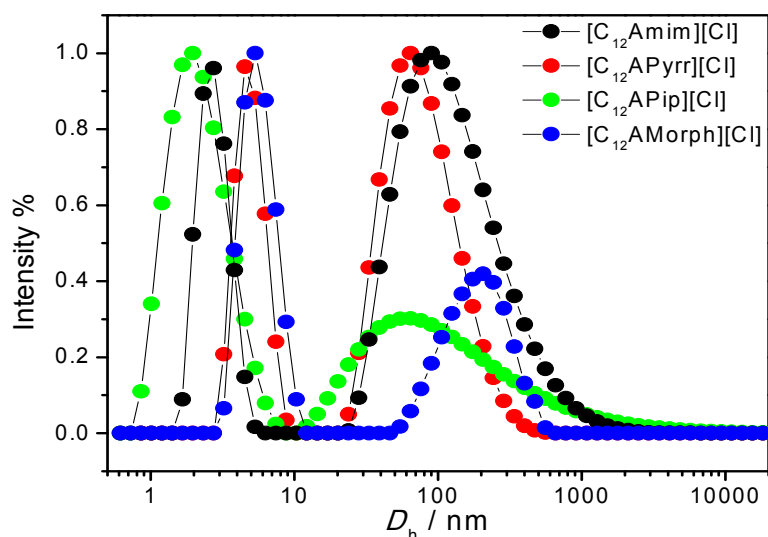
Figure 6: Intensity weighed hydrodynamic diameter (D_h) of micelles of different
SAILs in aqueous solutions at 298.15 K obtained from DLS measurements.

Therefore, the D_h corresponding to smaller micelles has been considered for further

discussion. The obtained D_h and polydispersity index of micelle is provided in Table S2

(supporting information). As can be seen from Figure 6, a D_h (at maximum scattering

intensity) in the range of 2.0-6.0 nm has been observed for micelles of different SAILs. The

D_h has been found to follow the order: $[C_{12}APip][Cl] < [C_{12}Amim][Cl] < [C_{12}APyrr][Cl] <$

$[C_{12}AMorph][Cl]$. The order signifies the dominating effect of van der Waal's volume of

cationic head group similar to that observed for variation of N_{agg} and β, where D_h increase with increase in size of cationic head group with the exception of [C$_{12}$AMorph][Cl].

Figure 7 (A-H) shows the AFM images (A-D), and corresponding 3D profiles (E-H) for micellar solutions of [C$_{12}$APip][Cl], [C$_{12}$APyrr][Cl], [C$_{12}$Amim][Cl] and [C$_{12}$AMorph][Cl], respectively.
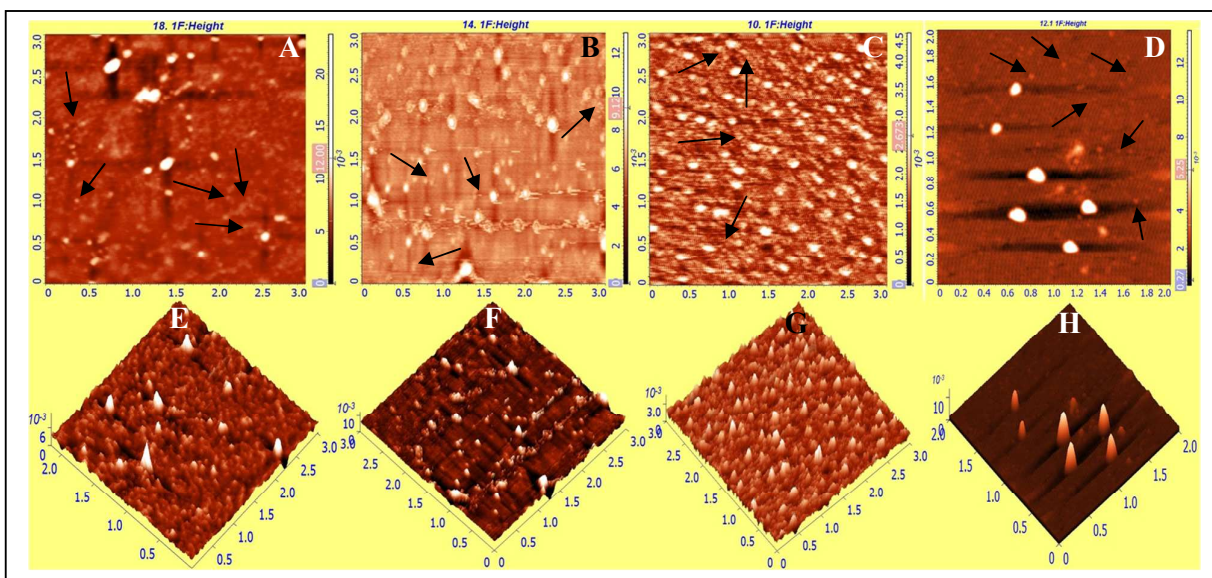
Figure 7 (A-F) AFM height profile (A-C) of aqueous micellar solutions of (A) [C$_{12}$AMim][Cl]; (B) [C$_{12}$AMorph][Cl]; (C) [C$_{12}$APip][Cl]; and (D) [C$_{12}$APyrr][Cl] as well as corresponding 3-D AFM-images of (E) [C$_{12}$AMim][Cl]; (F) [C$_{12}$AMorph][Cl]; (G) [C$_{12}$APip][Cl]; and (H) [C$_{12}$APyrr][Cl] at 298.15 K. A few arrows in Figure 6A-D are provided indicating the presence of smaller micelles as observed from DLS measurements however the presence of smaller micelles can be easily viewed in 3D images. In case of [C$_{12}$APyrr][Cl], it was difficult to land the probe during measurement, hence the sample could be imaged taken after several attempts.

AFM images (Figure 7A-D) show the presence of micelles of two sizes, one smaller and other larger. For better clarity, the smaller micelles in the height profiles (Figure 7A-D) are marked with arrows, however, they are relatively more visible in corresponding 3D images. The size of smaller micelles from AFM for investigated SAILs is in corroboration with the DLS measurements whereas the presence of larger micelles have been assigned to the agglomerates of the smaller micelles as also observed from DLS measurements. A careful examination of height profiles of respective AFM images (Figure 7 D-H) reveals that the

number of smaller micelles for all the SAILs under investigation is much more as compared to that of larger micellar agglomerates supporting the hypothesis. From 3D AFM profiles, it is clear that smaller micelles are spherical in shape, whereas the larger agglomerates are considered as non-spherical in nature. The presence of larger agglomerates may be due to the growth of the micelle at concentration of investigation.

Conclusion

The affect of variation of cationic head group on the micellization behavior of amide functionalized surface active ionic liquids (SAILs) has been investigated using a variety of state of art techniques. The functionalization of alkyl chain with amide group, prone to *H*-bonding, has been found to affect the micellization in a positive manner. The investigated SAILs have shown 3-4 fold lower *cmc* and better surface active properties as compared to their non-functionalized counterparts and conventional cationic surfactants owing to the presence of amide moiety. Further the relative hydrophobicity and size of the cationic head group has been found to affect the micellization behavior, where SAILs with large sized or relatively hydrophobic cationic head groups have shown better surface activity at air/solution interface and micellization behavior in bulk. Thermodynamics parameters obtained from isothermal titration calorimetry has indicated that the micellization of the investigated SAILs is an entropy driven phenomenon where the contribution of enthalpy change is relatively less. The size (D_h), aggregation number (N_{agg}) as well as compactness of micelle has been found to be in corroboration with each other. It is anticipated that the work reported here will prompt more researchers working in the field of aggregation of SAILs for functionalization of alkyl chain with other suitable functional groups to achieve much better surface active behavior.

Supporting Information

Detailed synthesis procedure. ^{1}H, ^{13}C NMR, ^{13}C DEPT, and mass spectral data of synthesized amide functionalized SAILs. Table S1 (size and PDI of micelles).

References

1. Poliakoff, M.; Fitzatrick, J. M.; Farren, T. R.; Anastas, P. T. *Science* **2002**, *297*, 807−810.

2. Chiappe, C.; Pieraccini, D. *J. Phys. Org. Chem.,* **2005**, *18*, 275−297.

3. Smiglak, M.; Metlen, A.; Rogers, R. D. *Acc. Chem. Res.,* **2007**, *40*, 1182−1192.

4. Rogers, D. R.; Seddon, R. K. *Science* **2003**, *302*, 792−793.

5. Welton, T. *Chem. Rev.,* **1999**, *99*, 2071-2084.

6. Dupont, J.; De Souza, R. F.; Suarez, P. A. Z. *Chem. Rev.,***2002**, *102*, 3667−3692.

7. Lee, S–g. *Chem. Commun.,* **2006**, *10*, 1049−1063.

8. Wasserscheid, P.; Keim, W. *Angew Chem., Int. Ed.,* **2000**, *39*, 3772−3789.

9. Wang, Y. T.; Voth, G. A. *J. Am. Chem. Soc.,***2005**, *127*, 12192–12193.

10. Lopes, J. N. A. C.; Padua, A. A. H. *J. Phys. Chem. B* **2006**, *110*, 3330–3335.

11. Lopes, J. N. C.; Gomes, M. F. C.; Padua, A. A. H. *J. Phys. Chem. B* **2006**, *110*, 16816–16818.

12. Triolo, A.; Russina, O.; Bleif, H. J.; Cola, E. D. *J. Phys. Chem. B* **2007**, *111*, 4641–4644.

13. Chamiot, B.; Rizzi, C.; Gaillon, L.; Sirieix-Ple´net, J.; Lelie`vre, J. *Langmuir* **2009**, *25*, 1311–1315.

14. Shi, L.; Li, N.; Zheng, L. *J. Phys. Chem. C* **2011**, *115*, 18295−18301.

15. Dong, B.; Zhang, J.; Zheng, L. Q.; Wang, S. Q.; Li, X. W.; Inoue, T. *J. Colloid Interface Sci.,* **2008**, *319*, 338−343.

16. Zhao, Y.; Gao, S. J.; Wang, J. J.; Tang, J. M. *J. Phys. Chem. B* **2008**, *112*, 2031−2039.

17. Bowers, J.; Butts, C. P.; Martin, P. J.; Vergara-Gutierrez, M. C. *Langmuir* **2004**, *20*, 2191−2198.

18. Wang, J. J.; Wang, H. Y.; Zhang, S. L.; Zhang, H. C.; Zhao, Y. *J. Phys. Chem. B* **2007**, *111*, 6181−6188.

19. Singh, T.; Kumar, A. *J. Phys. Chem. B* **2007**, *111*, 7843−7851.

20. Anderson, J. L.; Pino, V.; Hagberg, E. C.; Sheares, V. V.; Armstrong, D. W. *Chem. Commun.,* **2003**, *19*, 2444−2445.

21. Inoue, T.; Ebina, H.; Dong, B.; Zheng, L. Q. *J. Colloid Interface Sci.,* **2007**, *314*, 236−241.

22. Blesic, M.; Marques, M. H.; Plechkova, N. V.; Seddon, K. R.; Rebelo, L. P. N.; Lopes, A. *Green Chem.,* **2007**, *9*, 481−490.

23. Burns, C. T.; Lee, S.; Seifert, S.; Firestone, M. A. *Polym. Adv. Technol.,* **2008**, *19*, 1369−1382.

24. Blesic, M.; Swadzba-Kwasny, M.; Holbrey, D. J.; Lopes, N. C. J.; Seddon, R. K.; Rebelo, P. N. L. *Phys. Chem. Chem. Phys.,* **2009**, *11*, 4260−4268.

25. Li, X. -W.; Gao, Y. -A.; Liu, J.; Zheng, L. -Q.; Chen, B.; Wu, L. -Z.; Tong, C. -H.*J. Colloid Interface Sci., 2***010**, *343*, 94−101.

26. Wang, H.; Wang, J.; Zhang, S.; Xuan, X. *J. Phys. Chem. B* **2008**, *112*, 7843−7851.

27. Blesic, M.; Lopes, A.; Melo, E.; Petrovski, Z.; Plechkova, N. V.; Canongia Lopes, J. N.; Seddon, K. R.; Rebelo, L. P. N. *J. Phys. Chem. B* **2008**, *112*, 8645−8650.

28. Chauhan, V.; Singh, S.; Bhadani, A. *Colloids Surf. A* **2012**, *395*, 1−9.

29. Wang, X. Q.; Yu, L.; Jiao, J. J.; Zhang, H. N.; Wang, R.; Chen, H. *J. Mol. Liq.,* **2012**, *173*, 103−107.

30. Morrissey, S.; Pegot, B.; Coleman, D.; Garcia, M. T.; Ferguson, D.; Quilty, B.; Gathergood, N. *Green Chem.,* **2009**, *11*, 475−483.

31. Garcia, M. T.; Ribosa, I.; Perez, L.; Manresa, A.; Comelles, F. *Langmuir* **2013**, *29*, 2536−2545.

32. Kamboj, R.; Bharmoria, P.; Chauhan, V.; Singh, S.; Kumar, A.; Mithu, V. S.; Kang, T. S. *Langmuir* **2014**, DOI: 10.1021/la501897e

33. Wang, L.; Qin, H.; Wang, L.; Huo, S.; Zhao, B.; Song, B.; Yan, T. *J. Chem. Res.,* **2013**, 205−207.

34. Kamboj, R.; Singh, S.; Bhadani, A.; Kataria, H.; Kaur, G. *Langmuir* **2012**, *28*, 11969−11978.

35. Kamboj, R.; Singh, S.; Chauhan, V. *Colloids Surf. A* **2014**, *441*, 233−241.

36. Patra, D.; Barakat, C. *Spectrochimica Acta Part A* **2011**, *79*, 1823– 1828.

37. Patra, D.; Khoury, E. E.; Ahmadieh, D.; Darwish, S.; Tafech, R. M. *Photochemistry and Photobiology*, **2012**, *88*, 317–327.

38. Zhang, Q.; Gao, Z.; Xu, F.; Tai, S.; Liu, X.; Mo, S.; Niu, F. *Langmuir* **2012**, *28*, 11979−11987.

39. Hoque, J.; Kumar, P.; Aswal, V. K.; Haldar, V. *J. Phys. Chem. B* **2012**, *116*, 9718−9726.

40. Fredlake, P. C.; Crosthwaite, M. J.; Hert, G. D.; Aki, N. V. K. S.; Brennecke, F. J. *J. Chem. Eng. Data* **2004**, *49*, 954−964.

41. Arellano, I. H. J.; Guarino, J. G.; Paredes, F. U.; Arco, S. D. *J. Therm. Anal. Calorim.,* **2011**, *103*, 725−730.

42. Youns, N. M.; Mutalib, M. I. A.; Man, Z.; Bustam, M. A.; Murugesan, T. *J. Chem. Thermodyn.,* **2010**, *42*, 491−495.

43. Zhou. Z. B.; Matsumoto, H.; Tatsumi, K. *Chem. Eur. J.,* **2006**, *12*, 2196−2212.

44. Freire, M. G.; Neves, C. M. S. S.; Carvalho, P. J.; Gardas, R. L.; Fernandes, A. M.; Marrucho, I. M.; Luı́s M. N. B. F. Santos, L. M. N. B. F.; Coutinho, J. A. P. *J. Phys. Chem. B* **2007**, *111,* 13082−13089.

45. El Seoud, A. O.; Pires, A. R. P.; Abdel- Moghny, T.; Bastos, L. E. *J. Colloid Interface Sci.,* **2007**, *313*, 296−304.

46. Luczaka, J.; Hupkaa, J.; Thoming, J.; Jungnickel, C. *Colloids Surf. A* **2008**, *329*, 125−133.

47. Cornellas, A.; Perez, L.; Comelles, F.; Ribosa, I.; Manresa, A.; Garcia, M. T. *J. Colloid Interface Sci.,* **2011**, *355*, 164−171.

48. Quagliotto, P.; Barbero, N.; Barolo, C.; Artuso, E.; Barni, E.; Compari, C.; Fisicaro, E.; Viscardi, G. *J. Colloid Interface Sci.,* **2009**, *340*, 269−275.

49. Zhao, Y.; Yue, X.; Wang, X.; Huang, D.; Chen, X. *Colloids Surf. A* **2012**, *412*, 90−95.

50. Zhao, M.; Zheng, L. *Phys. Chem. Chem. Phys.,* **2011**, *13*, 1332−1337.

51. Rosen, M. J.; Mathias, J. H.; Davenport, L. *Langmuir* **1999**, *15*, 7340−7346.

52. Venable, L. R.; Nauman, V. R. *J. Phys. Chem.,* **1964**, *68*, 3498−3503.

53. Lah, J.; Pohar, C.; Vesnaver, G. *J. Phys. Chem. B* **2000**, *104*, 2522−2526.

54. Ray, B. G.; Chakraborty, I.; Ghosh, S.; Moulik, P. S.; Palepu, R. *Langmuir* **2005**, *21*, 10958−10967.

55. Anouti, M.; Jones, J.; Boisset, A.; Jacquemin, J.; Caillon-Caravanier, M.; Lemordant, D.; *J. Colloid Interface Sci.,* 2009, *340*, 104−111.

56. Shanks, C. P.; Franses, I. E. *J. Phys. Chem.,* **1992**, *96*, 1794−1805.

57. Bijma, K.; Engberts, J. B. F. N.; Blandamer, M. J.; Cullis, P. M.; Last, P. M.; Irlam, K. D.; Giorgio Soldi, L. *J. Chem. Soc., Faraday Trans.* **1997**, *93*, 1579−1584.

58. Li, Y.; Xu, R.; Couderc, S.; Bloor, D. M.; Wyn-Jones, E.; Holzwarth, J. F. *Langmuir* **2001**, *17,* 183−188.

59. Bouchemal, K.; Agnely, F.; Koffi, A.; Ponchel, G. *J. Colloid Interface Sci.,* **2009**, *338*,169−176.

60. Lah, J.; Pohar, C.; Vesnaver, G. *J. Phys. Chem. B* **2000**, *104,* 2522−2526.

61. Shimizu, S.; Pires, P. A. R.; El Seoud, O. A. *Langmuir*, **2004**, *20*, 9551−9559.

62. Faucompré, B.; Bouzerd, M.; Lindheimer, M.; Douillard, J. M.; Partyka, S. J. *Therm. Anal.* **1994**, *41*, 1325−1333.

63. Kalyanasundraram, K.; Thomas, K. J. *J. Am. Chem. Soc.,* **1977**, *99*, 2039−2044.

64. Turro, N. J.; Yekta, A. *J. Am. Chem. Soc.,* **1978**, *100*, 5961−5952.

65. Mandal, A. B.; Jayakumar, R. *J. Chem. Soc. Faraday Trans.*, **1994**, *90*, 161-165.

66. Bohren, C. F.; Huffman, D. R. Absorption and Scattering of Light by Small Particles, 530 pp., Wiley, New York, **1983**.